38th AIAA Fluid Dynamics Conference
23-26 June 2008, Seattle WA
AIAA-2008-3736

Boundary Layer Transition on X-43A

Scott Berry ,* Kamran Daryabeigi,† and Kathryn Wurster ‡
NASA Langley Research Center, Hampton, VA, 23681

and

Robert Bittner §
ATK Space Division, Hampton, VA, 23681

The successful Mach 7 and 10 flights of the first fully integrated scramjet propulsion systems by the Hyper-X (X-43A) program have provided the means with which to verify the original design methodologies and assumptions. As part of Hyper-X's propulsion-airframe integration, the forebody was designed to include a spanwise array of vortex generators to promote boundary layer transition ahead of the engine. Turbulence at the inlet is thought to provide the most reliable engine design and allows direct scaling of flight results to ground-based data. Pre-flight estimations of boundary layer transition, for both Mach 7 and 10 flight conditions, suggested that forebody boundary layer trips were required to ensure fully turbulent conditions upstream of the inlet. This paper presents the results of an analysis of the thermocouple measurements used to infer the dynamics of the transition process during the trajectories for both flights, on both the lower surface (to assess trip performance) and the upper surface (to assess natural transition). The approach used in the analysis of the thermocouple data is outlined, along with a discussion of the calculated local flow properties that correspond to the transition events as identified in the flight data. The present analysis has confirmed that the boundary layer trips performed as expected for both flights, providing turbulent flow ahead of the inlet during critical portions of the trajectory, while the upper surface was laminar as predicted by the pre-flight analysis.

Nomenclature

R_n	=	nose radius, in.
Re_θ	=	momentum thickness Reynolds number
M_e	=	edge Mach number
k	=	trip height, in.
δ	=	boundary layer thickness, in.
α	=	angle of attack, deg.
t	=	time from B-52 drop, sec.
T	=	surface temperature, deg-R

I. Introduction

NASA's Hyper-X (X-43A) program has successfully flown an airframe-integrated scramjet propulsion system at hypersonic conditions. Two flights have been achieved, one to Mach 7 and one to Mach 10. An overview of the pre-flight wind tunnel test program can be found in Ref. 1, 2, and 3, and flight results have recently been published in Ref. 4, 5, and 6. An artist's rendition of the X-43A vehicle in flight during the scramjet propulsion experiment is provided in Fig. 1a, while Fig. 1b provides a photograph of flight 2 during the boost stage for the first flight to Mach 7. This program has provided the first opportunity to obtain flight data on an autonomous hypersonic air-breathing propulsion system that is fully integrated with the vehicle airframe, and will validate/calibrate the

* Aerospace Engineer, Aerothermodynamics Branch, M/S 408A, AIAA Senior Member.
† Aerospace Engineer, Structural Mechanics & Concepts Branch, M/S 190, AIAA Senior Member.
‡ Aerospace Engineer, Vehicle Analysis Branch, M/S 451, AIAA Associate Fellow.
§ Aerospace Engineer, Hypersonic Air Breathing Propulsion Branch, M/S 168.

Figure 1a. Illustration of scramjet powered flight of Hyper-X

Figure 1b. Pegasus boost of Hyper-X vehicle to Mach 7

experimental, numerical, and analytical methods that were used for design and flight performance prediction. To reduce uncertainties associated with this cutting-edge technology maturation program prior to flight, a systematic and combined experimental and numerical approach was utilized. Technological advancements, required prior to flight, included development of aerodynamic performance and aeroheating databases, verification of performance and operability of the propulsion-airframe integration, and establishment of a method for boundary layer control. The present paper focuses on the development and use of boundary layer trips required as part of the engine inlet flow path. In order to provide the most robust scramjet propulsion system, the boundary layer approaching the scramjet inlet should be turbulent. Ingestion of a turbulent boundary layer increases inlet operability (by reducing susceptibility to flow separations within the engine) and therefore enhances overall engine performance. During the nominal flight condition, the location of natural transition on the Hyper-X forebody was estimated to be far beyond the inlet station based on "best estimates" of boundary layer transition for slender, planar configurations at hypersonic flight conditions (to be discussed in more detail). Thus, boundary layer trip devices were deemed necessary to ensure a turbulent boundary layer at the inlet for both Mach 7 and 10 flights. To develop boundary layer trips for the Hyper-X vehicle, a wind tunnel test program was initiated at the NASA Langley Research Center (LaRC), which is detailed in Ref. 7. The goal of the present paper is to present an analysis of the Hyper-X flight data, both in terms of the trip design and the natural transition measurements from the upper surface.

A. Hypersonic Boundary Layer Transition

As part of the fully integrated scramjet propulsion system, the lower surface forebody of the Hyper-X vehicle was designed to compress and process the flow going into the inlet. The lower surface forebody, see Fig. 2, is approximately 6-ft long and is characterized by a thin leading edge (R_n = 0.03-in for the Mach 7 vehicle, 0.05-in for Mach 10) and 3 flat ramps that provide a series of discrete, non-isentropic flow-compressions for the engine. At the nominal angle of attack of 2-deg (original design point for the Mach 7 vehicle, later changed to 2.5-deg), the first ramp provides an initial 4.5-deg of compression, followed by an additional 5.5-deg on the second ramp, and a final 3-deg of compression on the third ramp. Outboard of the flat ramps are the chines, which are designed to minimize three-dimensional effects and flow spillage. Ideally, the forebody would also provide a turbulent boundary layer for the inlet. A full-scale scramjet-powered vehicle, such as the National Aerospace Plane (NASP) or a similar derivative, would likely have sufficient forebody

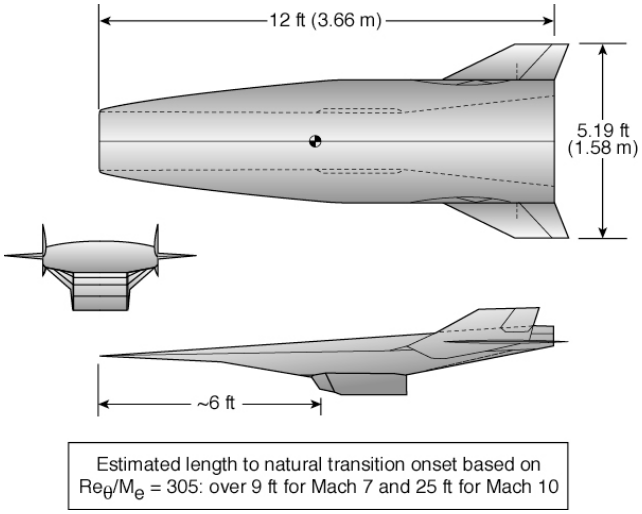

Figure 2. Hyper-X vehicle dimensions

length to provide a naturally turbulent boundary layer. As a sub-scale vehicle, Hyper-X requires forced boundary-layer transition in order to properly scale the engine flight test results to a future full-scale vehicle, as well as to the current ground-based data. While the primary emphasis is for the trips to provide turbulence for the inlet, a secondary goal is to alleviate the likelihood of a laminar separation at the first ramp corner, potentially promoting lateral flow spillage away from the inlet, thus reducing mass capture, and affecting performance.

An assessment of the Hyper-X forebody using the hypersonic boundary layer transition criteria developed during the NASP program[8] suggested that the vehicle forebody would be laminar at the nominal test condition.[9] Laminar values of the momentum thickness Reynolds number (Re_θ/M_e) for a sharp-nose wedge with 4.5-deg of turning were computed. The NASP sharp planar transition criterion of $Re_\theta/M_e = 305$ was used to estimate the onset of transition. For an initial assessment, this sharp planar criterion was deemed acceptable, as nose bluntness has a stabilizing influence that would further delay transition onset.[10] Based on this initial estimate, transition will not occur on the first ramp prior to the compression corner. In fact, over 200% more running length is required for transition to occur on the first ramp based on the accepted criterion, which is beyond the inlet. Thus, without a boundary layer trip, the potential exists for a laminar separation at the first ramp break that could generate some degree of lateral flow spillage. As for the question of transition prior to the inlet, a discrete compression corner is likely to promote transition (through instabilities within the separation/reattachment process), but to what degree is unknown. Very little ground based experimental data is available to provide guidance on forced transition through the use of discrete compression corners, and certainly less flight experience. To be conservative, the decision was made to force transition through the use of a passive (inert) trip array on the first ramp to ensure, at the very least, turbulent flow into the inlet, and also provide some flow spillage relief at the first ramp break.

B. Hyper-X Trips

The design of the Hyper-X trips was primarily predicated on empirical "rules-of-thumb" that were used to reduce the size of the experimental matrix. First, the general empirical design criteria dictated that the "tripping" mechanism most effective in forcing hypersonic transition required the formation of streamwise vorticity on a scale of the boundary layer height or less. Thus, the strategy was to create a series of counter rotating vortex pairs emanating from a spanwise array of trip elements, essentially vortex generators (VG), which were moderately smaller than the predicted boundary layer height. Initial analysis of the candidate trip configurations determined that, due to their relatively small size, the associated drag penalty to the vehicle would be minimal.[9] The placement of the array, downstream of the vehicle leading edge, was selected to be in the vicinity of a local Mach number at the boundary layer edge (M_e) of less than four.[11] While M_e rises rapidly near the leading edge, the first forebody ramp provides a wide domain of acceptable edge conditions. For both vehicles, the mid-point on the first ramp was selected as a compromise between locations close to the leading edge where M_e would be less and locations away from the leading edge where the sub-structure would be thicker and could easily accommodate the trip insert.

A lateral VG array on the first ramp of the Hyper-X lower surface forebody was selected as the approach for tripping the boundary layer for the Mach 7 and 10 flight vehicles. The boundary layer thickness was selected as the primary dimension with which to size and scale each unit-VG. Based on the ground-based data, a boundary layer trip height (k) over the boundary layer thickness (δ) of 0.6 was adequate to bring transition onset onto the first ramp and was utilized to size the Mach 7 flight vehicle trips, while a $k/\delta = 1.0$ was implemented for the Mach 10 vehicle.[7] This simple approach was deemed acceptable due to the ground-based data being at a similar length Reynolds number as flight.

Specifically, the approach taken to scale the wind tunnel results to flight was based on k/δ and included an assessment of the forebody boundary layer thickness for expected variations of the vehicle trajectory, angle-of-attack (α), and wall temperature (T_w) in flight. Mach 7 flight dispersions at the time of the trip design called for α = 2-deg ±1-deg and wall temperatures between 1000 and 1500°R. A maximum and minimum boundary layer thickness were computed from these dispersions and determined to be δ_{max} = 0.205-in and δ_{min} = 0.173-in. A trip height of k = 0.125-in provided an acceptable coverage of 60% to 70% of the boundary layer. This

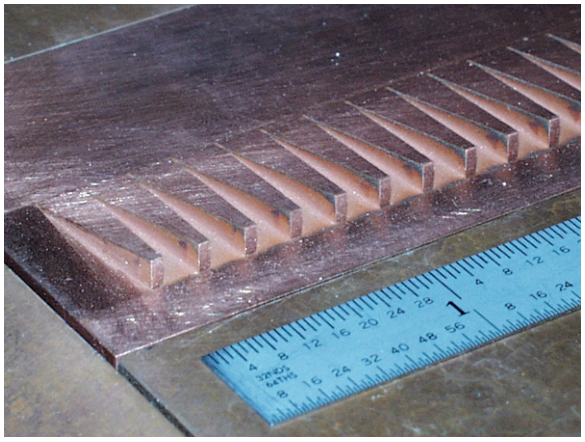

Figure 3. Close-up photograph of the boundary layer trips for Mach 7 flight

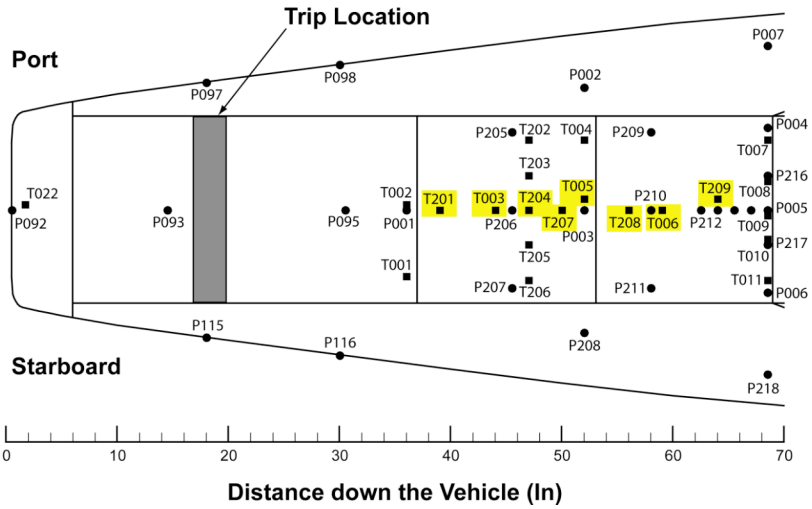

Figure 4. Lower forebody surface instrumentation layout for both flight vehicles

range was deemed adequate to force transition in a reasonably short distance behind the trip,[12] while not excessively enhancing the integrated closed-cowl heat load. Figure 3 provides a close-up photograph of the selected trip design, sized for the Mach 7 flight, installed on a full scale, prototype engine-vehicle (note the flow direction for this photo is roughly upper left to lower right). The successful flights now provide the unique opportunity to verify the trip design and the method by which the trip design was scaled to flight, as well as the natural transition criteria based on the upper surface results. A similar dispersion analysis was taken for sizing the final trips for the Mach 10 flight, except as stated before a k/δ of 1 was utilized based on the Mach 10 wind tunnel results. The trip geometry was scaled up from the Mach 7 design to be 0.26-in high, which allowed for acceptable coverage of 100% of the predicted boundary layer when the dispersions are considered.

II. Flight Instrumentation

A. Sensor Locations

Figures 4 and 5 illustrate the Hyper-X research vehicle upper and lower surface showing the location of pressure and temperature instrumentation for both vehicles. Details of the flight instrumentation can be found in Ref. 13. The thermocouples of interest for the present analysis are highlighted in yellow. On the lower surface, only the eight thermocouples along the centerline on the second and third ramps (T201, T003, T204, T207, T005, T208, T006, and T209) were considered, as these gauges were all imbedded thermocouples just slightly below the surface of the Shuttle-like TPS tiles. The two thermocouples on the first ramp (T022 and T002) were located on the tungsten ballast section, responding differently due to the heat absorption of the thermal mass and thus would have required a different thermal model in order to analyze the results. However, gauge T002 was monitored for

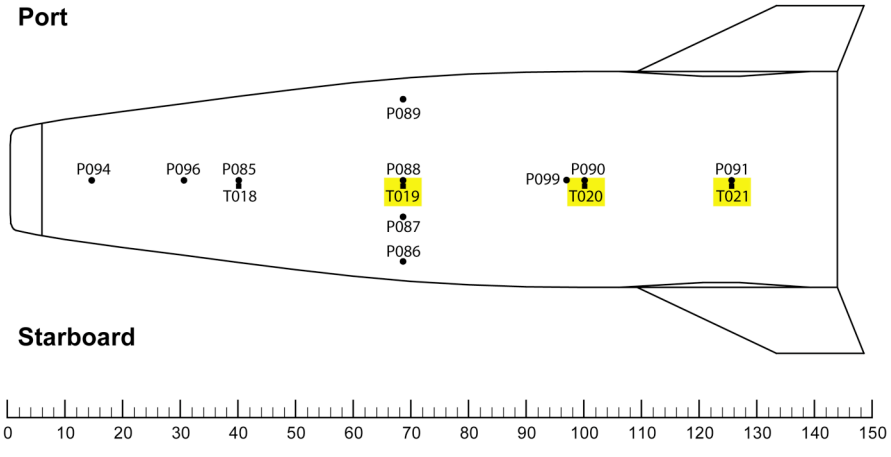

Figure 5. Upper surface instrumentation layout for both flight vehicles

indication of the local surface temperature along the Tungsten section for the boundary layer calculations, along with the first two gauges on the second ramp, T201 and T003. Also, the thermocouples shown in Fig. 4 towards the aft part of the forebody (T007 – T011) were also installed in a metallic region and for that reason were not analyzed for the present study. On the upper surface, Fig. 5, the three TPS-installed gauges along the centerline (T019, T020, and T021) were analyzed (T018 also was affected by the tungsten ballast).

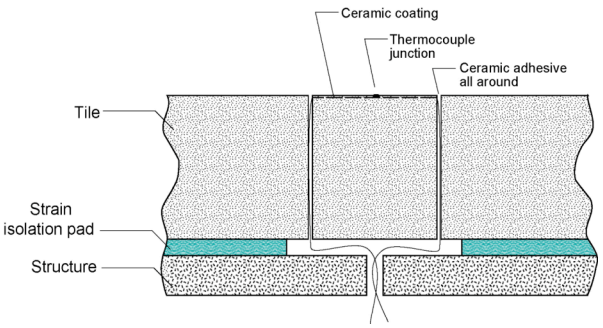

Figure 6. Typical thermocouple installation in TPS tile (from Ref. 13)

B. Thermocouple Installation

The surface temperatures were measured using 0.010-in diameter type-S thermocouples installed on the Alumina Enhanced Thermal Barrier (AETB) tiles. The range and accuracy requirement for these gauges were 490-3100°R and ±3°R, respectively. The AETB tiles, at a nominal density of 12 lb/ft^3, were 6 x 6-in with the thickness varying between 0.24 and 1.64-in depending on the tile location on the vehicle. The aerodynamic surface (or outer mold line) of each tile was coated with a diffusion layer made up of Toughened Uni-piece Fibrous Insulation (TUFI) and AETB, with a penetration depth of 0.1 inch. The tiles were bonded to a strain isolation pad (SIP) made of flexible reusable surface insulation (FRSI) material, and in turn bonded to the vehicle structure, using room temperature vulcanizing (RTV) silicone adhesive. Each thermocouple was mounted on the surface of a 0.75-in diameter AETB ceramic plug, which was installed in the middle of each tile as shown in Fig. 6. The ceramic plugs were coated with a high-emissivity putty material composed of crushed AETB material, borosilicate, an emissivity agent, and tetraorthosilicate (TEOS). The plugs were mounted flush to the surrounding tile surface. The manufacturer had suggested the nominal thickness of the coating on top of the thermocouple beads to be 0.002-in. Recent radiographic image analysis of a representative tile equipped with two instrumented plugs, and a more thorough evaluation of thermocouple installation procedures, suggested that the typical thermocouple bead depth was 0.010-in ± 0.005. The latter depth was used in the present analysis. The tile surfaces were also equipped with pressure ports for measuring the static surface pressure. The measured static pressures at locations close to thermocouple locations were used in conjunction with thermocouple data to obtain pressure and temperature dependent thermal properties required for deducing the heating rates from the measured temperatures. More detailed information on the tiles and thermocouples can be found in a preliminary report of the Mach 7 flight data.[14]

C. Thermal Properties

The thermal properties of SIP, RTV, aluminum and stainless steel were obtained from Williams and Curry.[15] Thermal properties of AETB-12 were obtained from Chiu and Pitts,[16] also available from the TPSX Material Properties Database (http://tpsx.arc.nasa.gov). No thermal or radiant properties were available for the high-emissivity coating applied on top of the AETB ceramic plugs, but the manufacturer had stated that the thermal and radiative response of the coating could be assumed to be similar to the reaction cured borosilicate glass (RCG) coating. RCG thermal and radiative properties[15] for the coating with a thermocouple depth of 0.002-in had been used in the preliminary report of Mach 7 flight data.[14] Further analysis of the constituents of the coating revealed that using RCG thermal properties is not justified. For the present study, AETB-12 thermal properties and RCG radiative properties were used for the coating, along with a thermocouple depth of 0.010-in. The temperature-dependent RCG emissivity data from Bouslog and Cunnington[17] were utilized.

III. Post-Flight Analysis

A. Heat Transfer Analysis

A one dimensional transient finite-volume numerical model was used to analyze heat transfer through the tiles and deduce the surface heating for each thermocouple location. A fully implicit (1st order accurate in time, 2nd order accurate in space) time marching formulation[18] was utilized. Previous aero-heating analysis of heating rates from measured surface temperatures on Space Shuttle Orbiter instrumented tiles had ignored the 0.015-in thick RCG coating in the thermal model and assumed that the measured thermocouple data were at the aerodynamic surface.[19] This assumption had not introduced significant error because of high thermal conductivity of RCG coating. For the present study, the coating was modeled in the thermal analysis. The first node was located on the aerodynamic

surface, and the second node at the thermocouple location (0.010-in below the surface). The measured temperature at node 2 and adiabatic conditions at the backface (structure) were used as the boundary conditions to obtain temperature distributions in the tile from node 3 to the structure at each instant of time. Then, fully implicit finite volume formulation of energy balances at nodes 2 and 1 were used to calculate the surface temperature and aero-heating rates at each time step, respectively. Additional details on the numerical heat transfer analysis can be found in Ref. 14.

1. Data Processing

The measured temperature and pressure data, recorded at 25 Hz, were subjected to two data processing procedures before proceeding to the heating analysis: spurious data removal, and smoothing, similar to the data processing used for calculating heating rates on the Space Shuttle Orbiter:[19] "Outlying" data points that were significantly different than the neighboring data points on either side, were replaced with preceding valid data points. A Hamming window filter[20] using a filter kernel length of 50, or 2 seconds of data, was used to smooth the recorded temperature and pressure data.

2. Uncertainty Assessment

Due to the limited number of thermocouples available, only 1-D (through the tile thickness) heat transfer was modeled in determining the heating rates. Lateral conduction due to the presence of surface heating gradients and material variations could lead to errors in the calculated heating rates from 1-D analysis.[21] The main sources of uncertainty considered in this study were due to the high-emissivity coating applied on top of the ceramic plugs, specifically the sensor depth and the thermal and radiative properties of the coating. The heating rate RMS uncertainties due to various sources of uncertainty were estimated to be: 3.5% due to the ±0.005 uncertainty in thermocouple depth, 15.1% due to use of AETB versus TUFI/AETB diffusion layer thermal properties for the coating, and 5.2% due to the use of temperature-dependent versus constant-temperature RCG emissivity. The overall RMS uncertainty in heating rates due to the combination of the individual sources of uncertainty was estimated to be 16.3%.

B. Engineering Analysis

An engineering code, MINIVER,[22] was utilized to assist in determining boundary layer transition times during the flight. MINIVER is a versatile engineering code that uses various well-known approximate heating methods, together with simplified flowfields and geometric shapes to model aeroheating environments for aerospace vehicles that operate in the hypersonic flight regime. MINIVER is suitable for research at the conceptual and preliminary design level, and is widely used by NASA, military, academic and commercial aerospace organizations throughout the U.S. The version of the code used for this study is the in-house NASA Langley version, which includes numerous operational advantages not available in the official government release, which was last updated in 1991.

Post-shock and local flow properties based on normal-shock or sharp-cone/wedge entropy conditions are determined in MINIVER through user selection of the various shock shape and pressure options. The calculations can be based on perfect-gas or equilibrium-air chemistry. Angle-of-attack effects are simulated either through the use of an equivalent tangent-cone or an approximate crossflow option[23]. The flow can be calculated for either two- or three-dimensional surfaces. However, the three-dimensional effects are available only through the use of the Mangler transformation for flat-plate to sharp-cone conditions. Over the last three decades, MINIVER has been used extensively as a preliminary design tool in government and industry and has demonstrated excellent agreement with more detailed solutions for stagnation and windward acreage areas on a wide variety of vehicle configurations, including the Space Shuttle Orbiter, HL-20,[24] X-33[25] (winged body, lifting body and vertical lander), X-34,[26] X-37,[27] X-43 and NASP. The principal advantage of this engineering code over some of the more detailed methods is the speed with which the analyses can be performed for each flow condition along a trajectory. Its strength lies in its ability to quickly provide the transient aeroheating environments required for TPS analysis and sizing.

In this investigation MINIVER was used to develop an estimate of the laminar and turbulent heating levels for a given body point along the best-estimated trajectory (BET) for each flight. Vehicle locations, on both the upper and lower surfaces, were modeled using Eckert flat plate heating methods,[28] Blasius skin friction (laminar) and Schultz-Grunow (turbulent) skin friction methods, and assuming wedge flow conditions at the equivalent angle of attack for each thermocouple (TC) location (8 lower surface and 3 upper surface). A radiation equilibrium temperature based on temperature-dependent emissivity data[17] was used as the wall temperature boundary condition. In addition to the fully laminar calculations, transition onset conditions were considered at the nose (0 in.), an approximate trip location (17 in.), and at the start of 2nd ramp (37.3 in.). A limited time-step sensitivity study was performed in order to ensure that the steep heating gradients were captured with minimal overshoot, resulting in a time-step interval selection of 0.25 sec, corresponding to the frequency of the thermocouple data. For the sake of discussion within

this paper, the MINIVER laminar and turbulent heating predictions will be used as guidance for determining the local boundary layer state by comparison to the reduced heating determined from the measured temperatures.

C. Computational Analysis & Assumptions

The boundary layer code of Clay Anderson,[29] which was originally used in the design of the boundary layer trips for flight,[12] was also used for the present analysis. The code was run with a simplified geometry (two-dimensional flat plates with sharp leading edge) and an input Mach number, free stream pressure, free stream temperature, and wall temperature. All computations were based on a fully laminar boundary layer. As a check, computations were run with the same inputs as the original design effort and the results were identical. The geometry utilized in this study was the vehicle centerline for the top and bottom surfaces of the X-43A configuration with the cowl closed. The bottom surface was only run to 37-in since that was sufficient to capture the boundary layer trips and the region downstream where tripping would occur. The boundary layer trip leading edge was at an axial location of 18.5-in (see Fig. 4). The top surface was run all the way to the vehicle base. All coordinate systems are based on Ref. 30.

As noted earlier, the present analysis utilizes the same methodology employed during the design of the flight trips. For the earlier effort, a simplifying assumption of modeling the leading edge as sharp was employed and then accounted for by comparison of the calculated boundary layer thickness from the boundary layer code to separate results obtained via viscous CFD solutions in which the leading edge bluntness was modeled (see Ref 12). For consistency, the same approach was employed here. Reference 31 provides for the Mach 7 case the details of the comparison between the three-dimensional Navier-Stokes (GASP) results and the present two-dimensional, sharp boundary layer code results, and only a summary discussion is included here. The comparison of the momentum thickness Reynolds number divided by the edge Mach number between the two computations showed nearly identical results over the first 30 inches of the vehicle, followed by slow departure of results with distance perhaps due to three-dimensional effects. On the other hand, the difference in boundary layer thickness was more significant, with as much as a 35% disagreement at the trip station. The present difference, a 0.050-in under-prediction by the boundary layer code, was nearly identical to the noted bluntness increment utilized previously during the design analysis. The conditions associated with the design analysis were different than the present comparison, and thus in both cases the difference between the CFD and boundary layer solutions are interpreted to be a direct result of bluntness. For the Mach 10 case a detailed analysis has not yet been completed, but preliminary results suggest that a total bluntness increment of 0.12-in is reasonable to account for both the sharp-to-blunt differences, as well as the late change in nose bluntness that occurred shortly before the flight.

On the upper surface, the local temperatures at each gauge were known based on the measured data. However, due to the limited spatial resolution of the temperature variation across the surface, the boundary layer analysis was conducted with a constant wall temperature. Also, the lower surface did not have gauges in the vicinity of the trips on the first ramp (tungsten section). For these reasons, wall temperature effects were assessed in the present analysis by computing results at a constant (and consistent) wall temperature of 800 °R as well as any noted range in measured surface temperatures (note: on the lower surface, T002 on the Tungsten was monitored). The computed variation based on the wall temperature range will be noted where appropriate either by discussion or with an uncertainty number in the figures.

IV. Mach 7 Flight Results

A. Temperature Measurements

Figure 9 provides the lower and upper surface temperature measurements for the centerline thermocouples during the first 500 seconds of the Flight 2 trajectory. Times are based on the release of the Hyper-X Launch Vehicle (Research Vehicle plus Pegasus booster) from the B-52. Separation from the booster occurred at approximately 92 seconds after drop, while cowl open and engine ignition was at roughly 96 seconds. On the lower surface, the measured temperatures all show roughly the same trends, all within a couple of hundred degrees of each other. The peak temperature measured on the lower surface was 2200°R for T208, which is near the

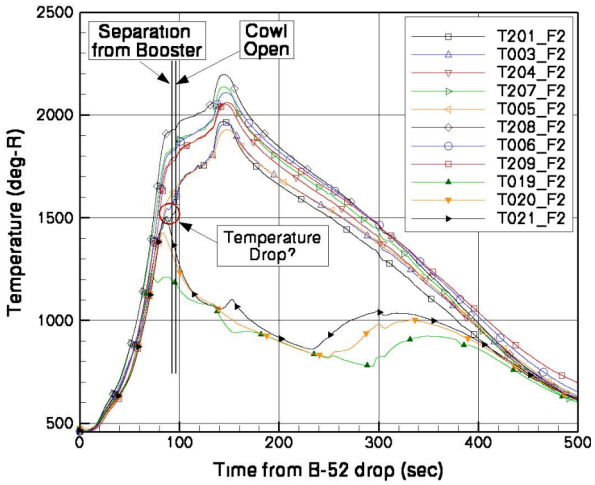

Figure 9. Surface temperature measurements for Hyper-X Flight 2

beginning of the third ramp. With the exception of the slight temperature deviation, in comparison to the others, for gauges T201 and T003 at around 80 seconds, the trends match exactly and might suggest the lower surface stayed turbulent during the entire trajectory. On the other hand, the upper surface showed a distinct and systematic departure from the quickly rising temperatures (initially of the same magnitude as the lower surface) that stabilized roughly around 1000°R before systematically increasing at around 250 seconds into the trajectory. This may be an indication that the upper surface was fully laminar during the powered scramjet portion of the trajectory.

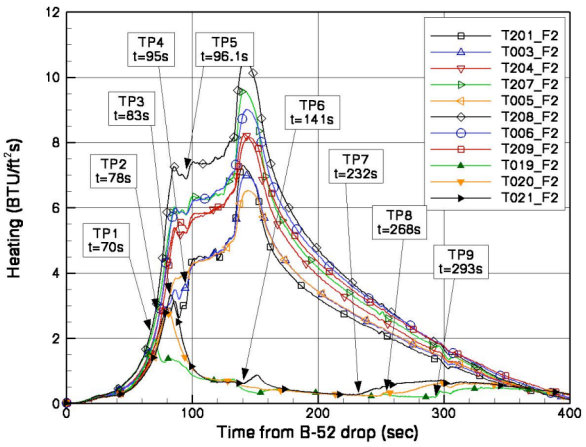

Figure 10. Reduced surface heating for Flight 2 of Hyper-X to Mach 7

B. Flight Heating Results

The results of the heating analysis for Flight 2, based on the assumptions and properties listed previously, are shown in Fig. 10 for both the lower and upper surfaces. Also plotted on this figure are proposed trajectory points identified for the subsequent boundary layer analysis, which were originally identified as part of a preliminary analysis detailed in Ref. 14. As mentioned previously with the temperature plots, the lower surface heating trends were all similar, with the exception of T201 and T003, which for a brief period of time between 78 and 95 seconds diverge noticeably from the others. These two times are identified in Fig. 10 as Trajectory Points 2 and 4. Also shown is Trajectory Point 5, an unclassified representative of the nominal test point (similar angle of attack and flow conditions but before the cowl opened). On the upper surface there is a systematic and precipitous drop in heating starting at 70 seconds (TP1) for thermocouple T019, and then at 83 seconds (TP3) for T021. The heating drop is interpreted as the end of turbulence for each location, and will be substantiated further in a following section. Conversely, later there is a systematic rise in heating, first starting with T021 at 232s (TP7), then T020 at 268s (TP8), and finally T019 at 293s (TP9), which is interpreted as the forward movement of transition onset. There is one other brief rise in the heating levels for T021 at 141s that also may be a transition event (TP6). Based on the present in-depth heating analysis, the deduced temperature at the surface had a peak value of 85.7°R higher than the measured flight thermocouple data plotted in Fig. 9 with a corresponding RMS deviation for the entire trajectory and all 11 thermocouples of 20.9°R.

C. Heating Level Assessment

As an initial guide to determining the state of the boundary layer during the Mach 7 flight, the reduced heating rates from the measured temperature response for each thermocouple were compared against the corresponding MINIVER predictions as a function of time from the B-52 drop. Two representative comparisons are provided in

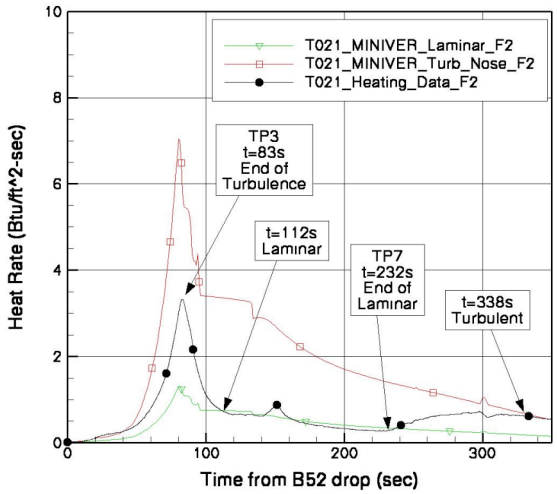

Figure 11. Comparison of reduced T021 heating to MINIVER predictions for Mach 7 flight

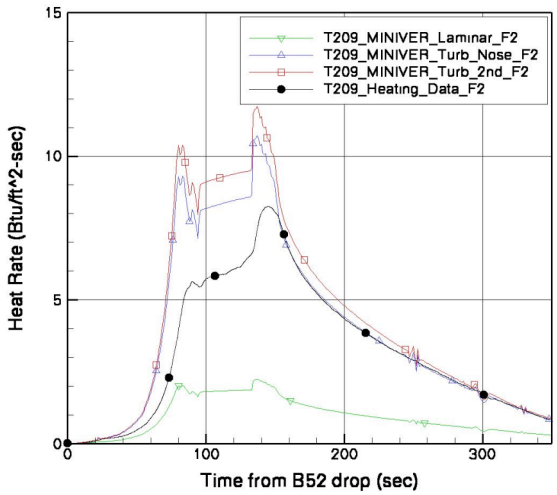

Figure 12. Comparison of reduced T209 heating to MINIVER predictions for Mach 7 flight

Figs. 11 and 12, for the upper and lower surfaces, respectively. For the upper surface, the heating results for T021 initially appear to be closer to the MINIVER calculated turbulent heating profile (for an assumed all-turbulent case with transition at the nose), and then drops down to the all-laminar calculated profile. The departure point is shown in Fig. 11 to be 83s, which was previously identified as the end of turbulence (or onset of laminar) point and the time at which the heating level appears all laminar is 112s. The departure from the laminar predicted profile is also shown to be 232s, with fully turbulent conditions at 338s. For the lower surface, Fig. 12, the reduced heating profile appears to be closer to the predicted turbulent heating results from MINIVER for most of the trajectory. Note that for the lower surface, turbulent predictions were completed for both fully turbulent from the nose and transition starting at the start of the second ramp.

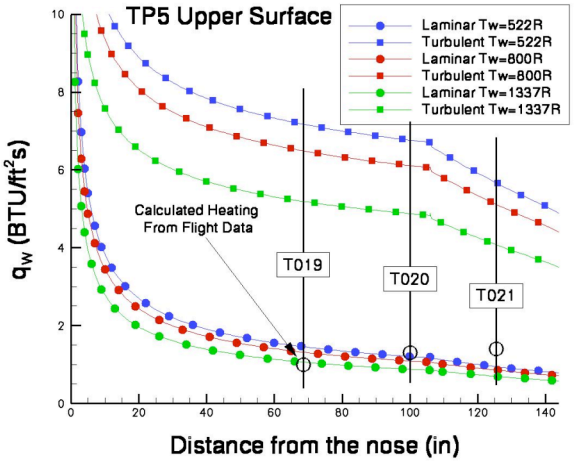

Figure 13. Comparison of Mach 7 flight heating rates to BL code predictions

A further comparison of the reduced heating rates from the flight data to the predicted laminar and turbulent heating (now based on the boundary layer code results) for TP5, for the range of measured temperatures on the upper surface, are shown in Fig. 13. As can be seen with this comparison, the heating rates for the upper surface at t=96s are in close agreement with laminar predictions from the boundary layer code. Note that the rising trend in flight heating rates are due to the aft gauges still not having fully recovered from turbulent conditions, which for T021 is at 112s (see Fig. 11). Knowing that the upper surface is laminar at the nominal test point anchors the rest of the trajectory points, as TP1 and TP3 would similarly have to correspond to the end of turbulence for the upper surface, while TP7 through TP9 would represent transition onset during descent. At the same time the lower surface heating rates (Fig. 10) are on the order 5 to 6 times higher than the laminar values on the upper surface and are shown to be similar to the predicted turbulent levels from MINIVER (Fig. 12). Thus, the evidence tends to support that the lower surface (with the possible exception of T201 and T003 for the brief period between TP2 and TP4) remained turbulent during the entire trajectory, while the upper surface was laminar for over a 120 seconds (including the powered scramjet portion) of the trajectory. Note that this determination of the boundary layer state is based on the comparisons to the laminar and turbulent *trends* from MINIVER and not the absolute values.

D. Trajectory Information

The trajectory points of interest (for the subsequent calculation of boundary layer properties), with the times previously identified from the heating plots, are now established in Figs. 14 and 15 during ascent and descent, respectively. The figures do not include any "real" trajectory information during the open cowl (classified) portion

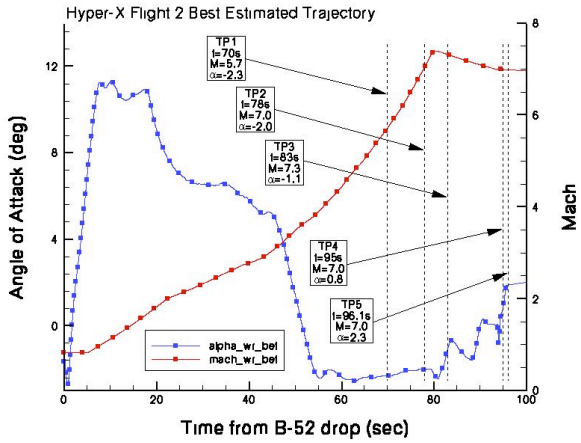

Figure 14. Mach 7 trajectory points for boundary layer analysis on ascent

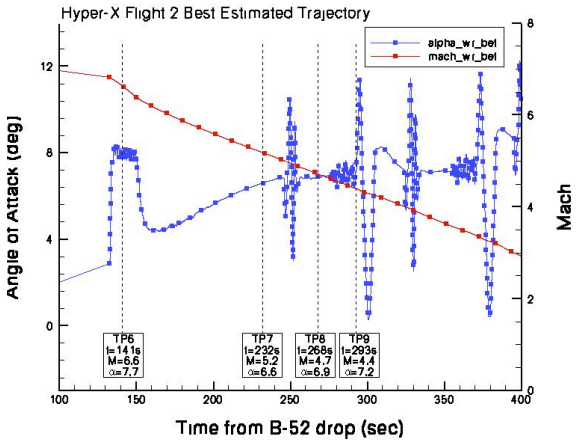

Figure 15. Mach 7 trajectory points for boundary layer analysis on descent

of the trajectory, but instead shows a straight line connecting the two unclassified sections. Descriptions of the underlying basis for each of the nine trajectory points are described in Table 1, along with key flow conditions associated with each as determined from the Best Estimated Trajectory (BET) v2.3.[32] Note that the version number denotes that this trajectory is the third (and most recent) release of the BET for the second flight. There are four ascent points (two each based on the upper and lower surface), one point just before the cowl opens (representing the "unclassified" test point), and four descent points (all based on the upper surface). Times are listed referenced to the sensed drop of the Hyper-X Launch Vehicle.

Table 1. Mach 7 trajectory points for boundary layer analysis

Trajectory Point	Time (sec.)	α (degrees)	Mach	Surface: Event Description
1	70	-2.317	5.719	Upper: T019 indicates laminar onset?
2	78	-2.038	7.040	Lower: T201& T003 appear non-turbulent?
3	83	-1.077	7.318	Upper: T021 indicates laminar onset?
4	95	0.844	6.989	Lower: T201 & T003 return to turbulent?
5	96.1	2.329	6.975	Lower: Approximate nominal angle of attack
6	141	7.684	6.639	Upper: T021 shows heating rise?
7	232	6.593	5.185	Upper: T021 indicates transition onset?
8	268	6.881	4.720	Upper: T020 indicates transition onset?
9	293	7.199	4.397	Upper: T019 indicates transition onset?

Mach 10 Flight Results

A. Temperature Measurements

Figure 16 provides the lower and upper temperature measurements for the centerline thermocouples during the first 800 seconds of the Flight 3 trajectory. Times again are based on the release of the Hyper-X Launch Vehicle from the B-52. Separation from the booster occurred at approximately 88 seconds after drop, while cowl open and engine ignition was at roughly 92 seconds. On the lower surface, most of the measured temperatures all show roughly the same trends, all within a couple of hundred degrees of each other, except for T201 (the furthest forward sensor) which seems to display a different behavior. The peak temperature measured on the lower surface was 2880°R for T006, which is near the beginning of the third ramp. All of the sensors, both upper and lower, appear to suggest significant temperature fluctuations that begin at around 80 seconds, after which most of the lower surface temperatures appear to rise sharply while the upper surface temperatures decrease slightly. As mentioned earlier, T201 is an outlier that takes a while (until about 276s) to reach the same trends as the other lower surface sensors. Similar to the Mach 7 flight, the upper surface for the Mach 10 flight shows a distinct and systematic departure from the quickly rising temperatures (initially of the same magnitude as the lower surface) that stabilizes roughly around

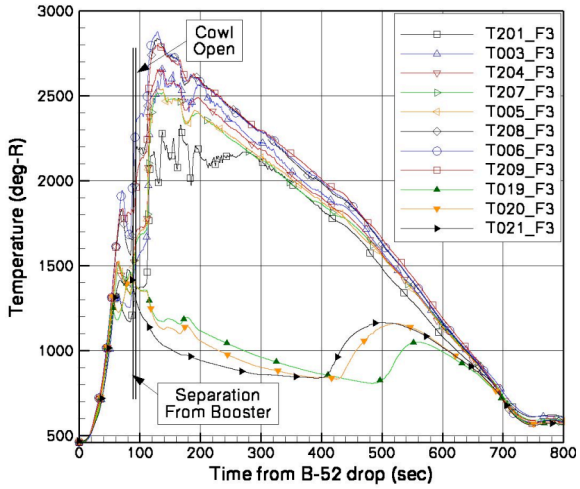

Figure 16. Surface temperature measurements for Hyper-X Flight 3

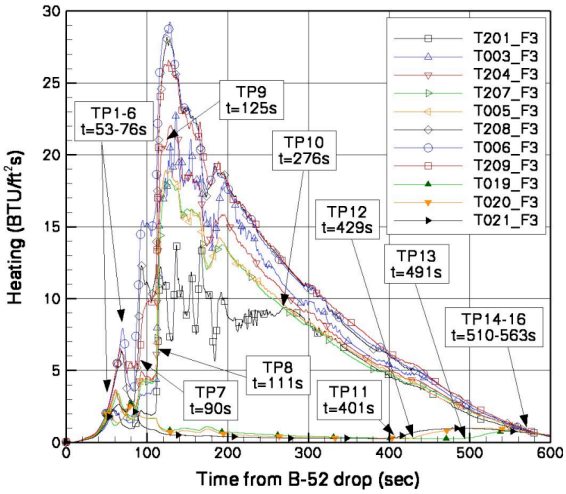

Figure 17. Reduced surface heating for Flight 3 of Hyper-X to Mach 10

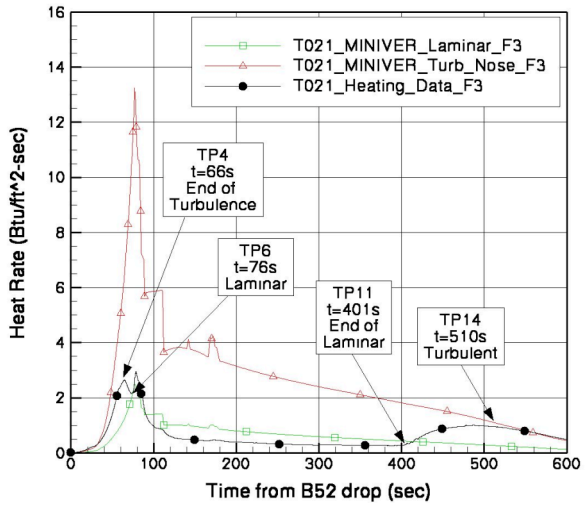

Figure 18. Comparison of reduced T021 heating to MINIVER predictions for Mach 10 flight

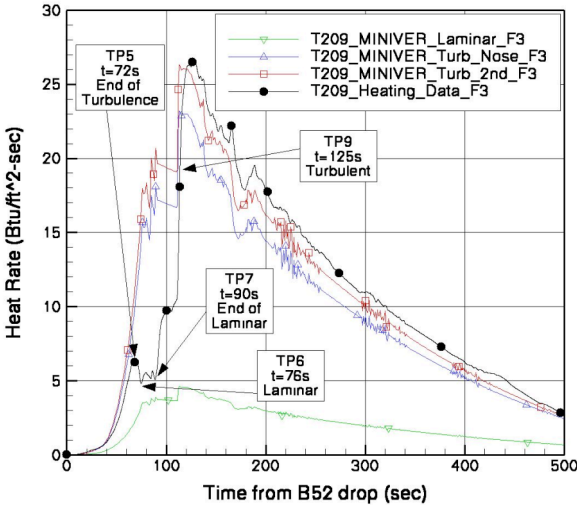

Figure 19. Comparison of reduced T209 heating to MINIVER predictions for Mach 10 flight

1000°R before systematically increasing at around 400 seconds into the trajectory. This suggests that the upper surface was fully laminar during the powered scramjet portion of the trajectory. The lower surface, however, is a little harder to interpret based on the measured temperatures.

B. Flight Heating Results

The results of the heating analysis for Flight 3 (Mach 10), consistent with the assumptions and properties of the Mach 7 case, are shown in Fig. 17 for both the lower and upper surfaces. Also plotted on this figure are proposed trajectory points identified for the subsequent boundary layer analysis. As mentioned previously with the temperature plots, the lower surface heating trends were all similar, with the exception of T201, which for a period of time between 55 and 276 seconds diverge noticeably from the others. These two times are identified in Fig. 17 as Trajectory Points 2 and 10. Also shown is Trajectory Point 7, an unclassified representative of the nominal test point (similar angle of attack and flow conditions but before the cowl opened). On the upper surface there is a systematic and precipitous drop in heating starting at 53 seconds (TP1) for thermocouple T019, and then at 66 seconds (TP4) for T021. The heating drop is interpreted as the end of turbulence for each location, and will be substantiated further in a following section. Conversely, later there is a systematic rise in heating, first starting with T021 at 401s (TP11), then T020 at 429s (TP12), and finally T019 at 491s (TP13), which is interpreted as the forward movement of transition onset. All of the sensors show a significant drop in the heating levels between 55 and 90 seconds (TP2 – TP7), which could indicate that the lower surface was briefly laminar. Based on the present in-depth heating analysis, the deduced temperatures at the surface was at most 165.8°R higher than the measured flight thermocouple data plotted in Fig. 16 with a corresponding RMS deviation for the entire trajectory and all 11 thermocouples of 24.2°R.

C. Heating Level Assessment

Again, the reduced heating rates from the measured temperature response for each thermocouple were compared against the corresponding MINIVER prediction as a function of time from the B-52 drop in order to determining the state of the boundary layer during the Mach 10 flight. Three representative comparisons for the upper and lower surfaces are provided in Figs. 18 - 20. In this case two lower surface comparisons are provided to help classify the boundary layer status close to the trip station (T201) and close to

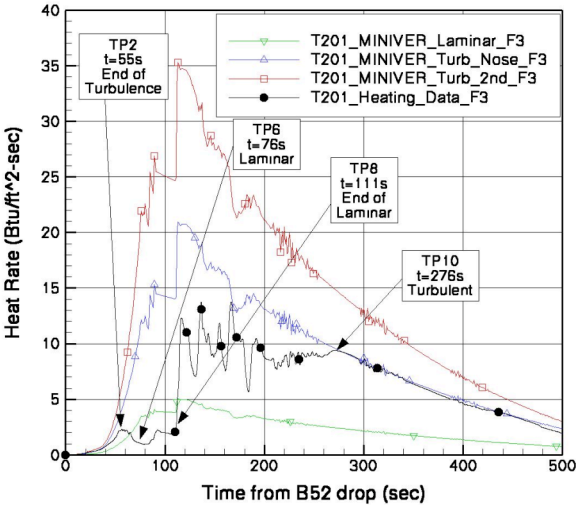

Figure 20. Comparison of reduced T201 heating to MINIVER predictions for Mach 10 flight

the engine inlet (T209). For the upper surface, the heating results for T021 initially are closer to the MINIVER calculated turbulent heating profile (for an assumed all-turbulent case with transition at the nose), and then drops down to the all-laminar calculated profile. The departure point is shown in Fig. 18 to be 66s (TP4), which was previously identified as the end of turbulence (or onset of laminar) point and the time at which the heating level appears all laminar is 76s (TP6). The departure from the laminar predicted profile is also shown to be 401s (TP11), with fully turbulent conditions at 510s (TP14). For T209 on the lower surface, Fig. 19, the reduced heating is also initially close to the predicted turbulent heating results from MINIVER, with an abrupt departure at 69s that plateaus at a laminar-like level at 75s. The surface heating then increases, starting at 90s, to the same level of the turbulent MINIVER predictions at 125s. For T201 on the lower surface, Fig. 20, the departure from the turbulent levels occurs at 55s, reaches laminar levels at 82s, and then a sharp rise towards the turbulent predictions starts at 110s, but does not reach the turbulent profile until 276s. The times identified in Figs. 19 and 20 should provide the information needed to identify the boundary layer conditions associated with the trips being fully effective and incipient.

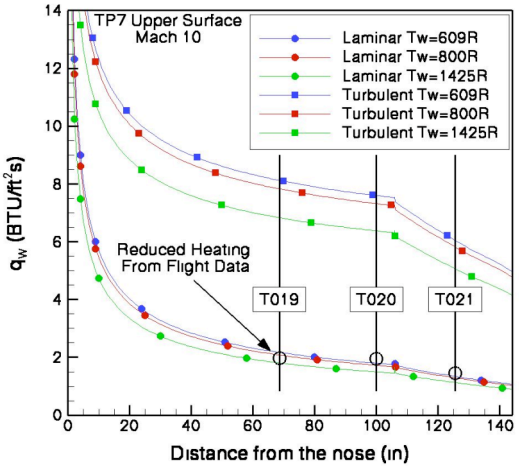

Figure 21. Comparison of Mach 10 flight heating rates to BL code predictions

Figure 21 provides a comparison of the reduced heating rates from the flight data to the laminar and turbulent heating predicted from the boundary layer code for TP7 for the range of measured temperatures on the upper surface. As can be seen with this comparison, the heating rates for the upper surface at 90s are in close agreement with laminar predictions from the boundary layer code. Again, with the knowledge that the upper surface is laminar at the nominal test point anchors the rest of the trajectory points, as TP1 and TP2 would have to correspond to the end of turbulence for the upper surface on ascent, while TP11 through TP13 would represent transition onset during descent. For the lower surface, the heating rates (Fig. 17) at 90s are only on the order 2 times higher than the laminar values on the upper surface and are shown to also be laminar levels (or nearly so) from MINIVER (Fig. 19). Thus, the evidence suggests that the lower surface was briefly laminar, or at least not turbulent, just in front of the inlet between 69s and 90s (which is just prior to the engine cowl opening), and transitional during the engine test. The upper surface was laminar for over 325 seconds (including the powered scramjet portion) of the trajectory.

D. Trajectory Information

The trajectory points of interest, with the times previously identified from the heating plots, are now established in Figs. 22 and 23 during ascent and descent, respectively. The figures do not include any "real" trajectory information during the open cowl (classified) portion of the trajectory, but instead shows a straight line connecting

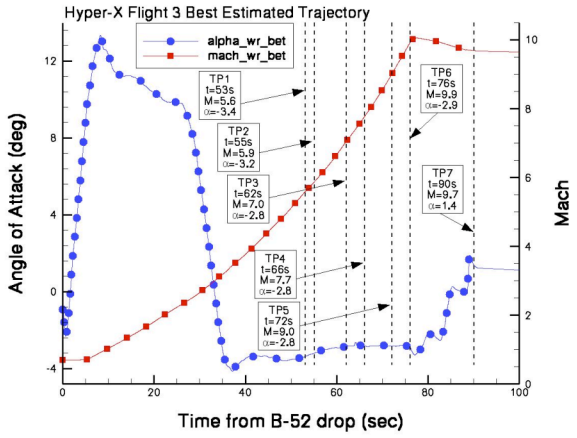

Figure 22. Mach 10 trajectory points for boundary layer analysis on ascent

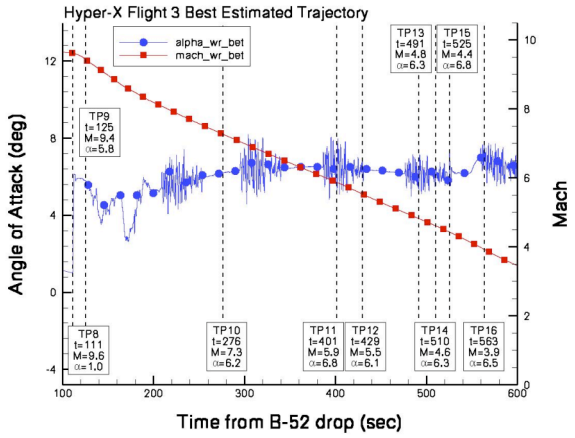

Figure 23. Mach 10 trajectory points for boundary layer analysis on descent

the two unclassified sections. Descriptions of the underlying basis for each of the 16 trajectory points are described in Table 2, along with key flow conditions associated with each as determined from the BET v3.1.[33] Note that the version number denotes that this trajectory is the first release of the BET for the third flight. There are six ascent points, one point just before the cowl opens (representing the "unclassified" test point), and nine descent points.

Table 2. Mach 10 trajectory points for boundary layer analysis

Trajectory Point	Time (sec.)	α (degrees)	Mach	Surface: Event Description
1	53	-3.38	5.57	Upper: T019 turbulent to laminar
2	55	-3.21	5.86	Both: T020 & T201 turbulent to laminar
3	62	-2.85	7.03	Upper: T019 laminar
4	66	-2.83	7.75	Upper: T020 laminar & T021 turbulent to laminar
5	72	-2.83	8.98	Lower: T209 turbulent to laminar
6	76	-2.86	9.90	Both: T021, T201, T209 laminar
7	90	1.40	9.69	Lower: T209 laminar to turbulent
8	111	1.01	9.62	Lower: T201 laminar to turbulent
9	125	5.79	9.44	Lower: T209 turbulent
10	276	6.19	7.27	Lower: T201 turbulent
11	401	6.79	5.87	Upper: T021 laminar to turbulent
12	429	6.10	5.54	Upper: T020 laminar to turbulent
13	491	6.32	4.82	Upper: T019 laminar to turbulent
14	510	6.29	4.61	Upper: T021 turbulent
15	525	6.81	4.43	Upper: T020 turbulent
16	563	6.48	3.91	Upper: T019 turbulent

V. Boundary Layer Analysis

A. Natural Transition (Upper Surface) Results

Figure 24 shows a plot of Re_θ/M_e as a function of axial distance for the three trajectory points that relate to the top surface during the Mach 7 ascent. The plot indicates the gauge locations via vertical bars with gauge numbers listed. The wall temperatures utilized were based on the range of measured values on the upper surface at that point on the trajectory. These trajectory points were identified based on the data suggesting the boundary layer was beginning to transition from turbulent to laminar, which provided Re_θ/M_e of 453 for TP1, 420 for TP2, and 393 for TP3. The measured variation in upper surface wall temperatures provides less than a 4% change in the calculated values of Re_θ/M_e. Since during these particular trajectory points the vehicle is experiencing some rapid changes in angle of attack and flow conditions, a sensitivity study to small increments in time around TP1 and TP3 was performed. Reference 31 provides the details of that analysis, where a one or two second shift in time for each trajectory point was enough to adjust the results such that these cases overlapped at a value of Re_θ/M_e of 400. Typically a value of 300 is expected for boundary layer transition onset from laminar to turbulent. Note that TP2 also corresponds to when T019 indicated the start of laminar flow, which provided a lower value of Re_θ/M_e (~350).

Figure 25 shows a similar plot of Re_θ/M_e as a function of axial distance for the trajectory points that relate to the

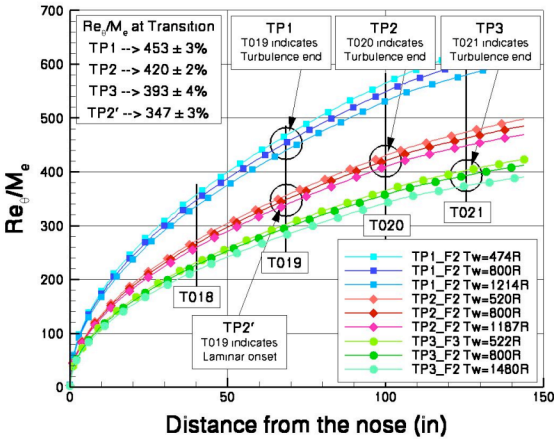

Figure 24. Upper surface Re_θ/M_e for Mach 7 Trajectory Points 1 - 3

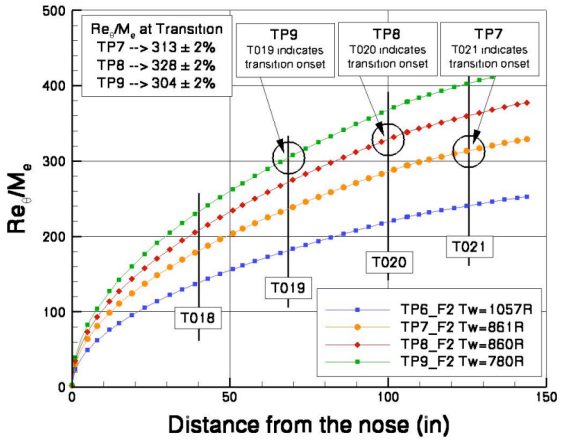

Figure 25. Upper surface Re_θ/M_e for Mach 7 Trajectory Points 6 - 9

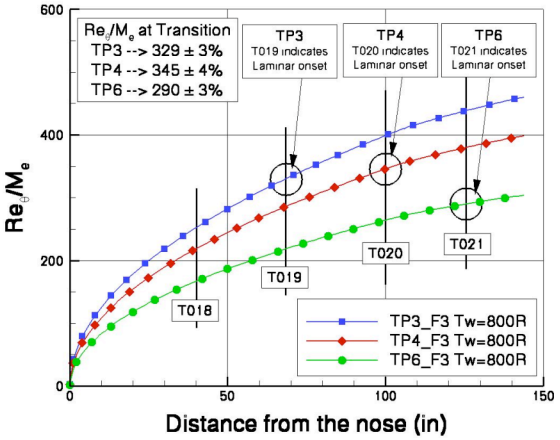

Figure 26. Upper surface Re_q/M_e for Mach 10 ascent trajectory points

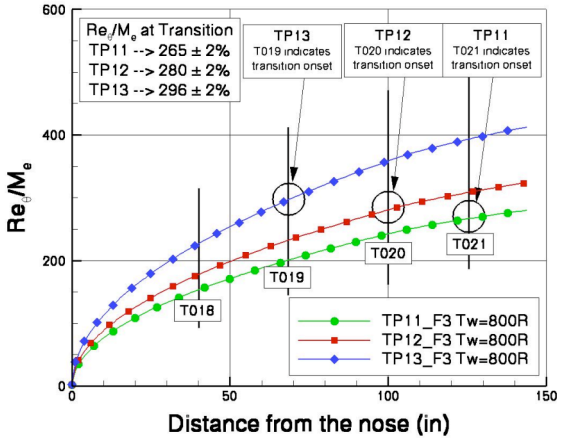

Figure 27. Upper surface Re_q/M_e for Mach 10 descent trajectory points

top surface but now during Mach 7 descent. The wall temperature shown was based on the measured value at that location at that point in the trajectory, while the uncertainty variance listed in the figure is based on the range of temperatures on the upper surface. In this case an approximate value of 300 seems appropriate for transition onset from laminar to turbulence, roughly validating the pre-flight transition criteria for transition onset. The actual values predicted were 313 for trajectory point 7, 328 for trajectory point 8, and 304 for trajectory point 9, with roughly a 2% uncertainty spread based on wall temperature. These results indicate that the NASP transition criterion was sufficient to indicate transition from laminar to turbulent flow. Trajectory point 6, which indicated a brief increase in the heating rates, only had a Reynolds number ratio of 240 and probably was not a transition event, but instead related to the high angle of attack maneuver shown in Fig. 15.

Figure 26 shows a similar plot of Re_θ/M_e as a function of axial distance for the three trajectory points that relate to the top surface sensor locations first indicating laminar conditions during the Mach 10 ascent. The wall temperatures shown are based on the nominal value for each trajectory point. These trajectory points were identified based on the data suggesting when the boundary layer was first laminar, which provided Re_θ/M_e of 329 for TP3, 345 for TP4, and 290 for TP6. The measured variation in upper surface wall temperatures provides at most a 4% change in the calculated values of Re_θ/M_e. For the trajectory points for which these sensors first showed the departure from turbulent heating rates (TP1, TP2, and TP4), a higher value of Re_θ/M_e, roughly 400, was identified (not shown).

Figure 27 shows a similar plot of Re_θ/M_e as a function of axial distance for the trajectory points that relate to the top surface but now during Mach 10 descent. The calculations shown are based on the nominal wall temperature for each trajectory point. In this case an average value of 280 seems appropriate for the onset of transition from laminar to turbulence, which again is slightly lower than the corresponding result during ascent. These Mach 10 descent results are similar to the results identified with the Mach 7 flight data. The actual values predicted were 265 for TP11, 280 for TP12, and 296 for TP13, with roughly a 2% uncertainty spread based on wall temperature. These results also indicate that the NASP transition criterion is a reasonable approach for estimating the onset of natural transition from laminar to turbulent flow at hypersonic flight conditions.

B. Forced Transition (Lower Surface) Results

Figure 28 shows a plot of the momentum thickness Reynolds number over edge Mach number ratio as a function of axial distance for the Mach 7 trajectory points that relate to the bottom surface (also including TP3). For this comparison, a consistent wall temperature of 800°R was utilized for each trajectory point. Although not included on the plot, when the range of measured surface temperatures were

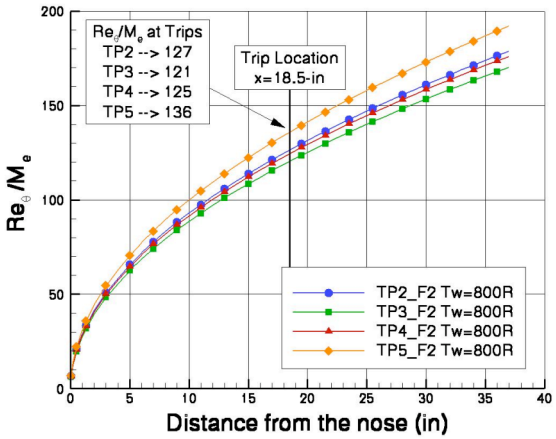

Figure 28. Lower surface Re_q/M_e at trips for the Mach 7 trajectory points

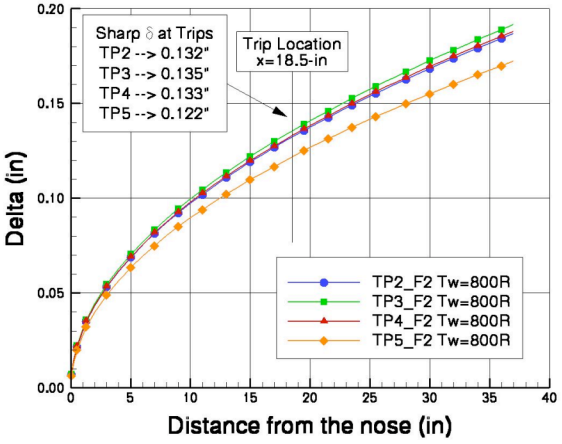

Figure 29. Boundary layer thickness calculations for the Mach 7 lower surface

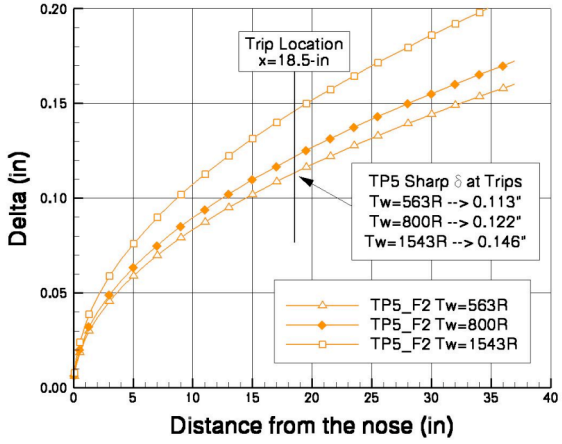

Figure 30. Boundary layer thickness sensitivity to temperature variations for Mach 7 lower surface

investigated, only a 3% difference in Re_θ/M_e was noted. Of the trajectory points selected, TP2 and TP4 correspond to when gauges 201 and 003 indicate the beginning and end to brief reduction in heating (interpreted as a reduction in tripping effectiveness), while TP3 represented a trajectory point in between where the effectiveness was the least. TP5 was selected as the unclassified representative of the nominal design point for comparison to the pre-flight predictions. The actual values predicted at the trip location were 127, 121, 125, and 136 for trajectory points 2, 3, 4, and 5, respectively. The lowest computed value of Re_θ/M_e was for TP3, which qualitatively agrees with the reduced tripping effectiveness trends, while the end points TP2 and TP4 have roughly the same value. Compared to the pre-flight natural transition criterion (Re_θ/M_e = 305 from NASP), the local values for all four trajectory points were roughly a factor of three less than that required for natural transition and thus the first ramp (at the very least) would have likely been laminar, with the resulting laminar separation at the ramp corner, during much of the high Mach number portion of the flight 2 trajectory.

The boundary layer thickness is plotted in Fig. 29 for the same four Mach 7 lower-surface trajectory-points of interest. Once again the values at trajectory points 2 and 4 are about the same at the trip location. For the on-design case (TP5), the boundary layer thickness was calculated to be 0.122-in for a wall temperature of 800 °R. As stated earlier, the flight trips were sized to have a minimum height of 60% of the boundary layer thickness[34] considering a two-degree span of angle of attack and additional increments for wall temperature effects and bluntness. The original analysis resulted in a thickness of 0.182-in for the then-nominal angle of attack of 2-deg with bluntness at a wall temperature of 1000°R and the resultant trip height was 68% of the boundary layer thickness. Utilizing the bluntness increment (mentioned previously) of 0.050-in with the calculated boundary layer thickness for TP5 results in an estimated thickness of 0.172-in, or k/δ of 0.73. The actual test point angle of attack increased from 2.0 to 2.3-deg (the closest angle of attack case with the cowl closed), however the resulting boundary layer thickness was offset by the measured wall temperature being lower than predicted. Figure 30 shows the sensitivity of boundary layer thickness to wall temperature. Using the measured temperature at gauge T201 to represent the first ramp, which is not realistic but gives an upward bound, results in a sharp-value boundary-layer thickness of 0.146-in, and with the bluntness increment, 0.192-in. The tungsten section temperature measurement from gauge T002, which is a little low when compared to the pre-flight predictions (perhaps due to its proximity to the ramp corner), results in the lower bound thickness of 0.113-in, or 0.159-in with bluntness. Thus, the range of boundary layer thicknesses (including bluntness) corresponding to the range of potential surface temperatures at the trip station is 0.159-in to 0.192-in,

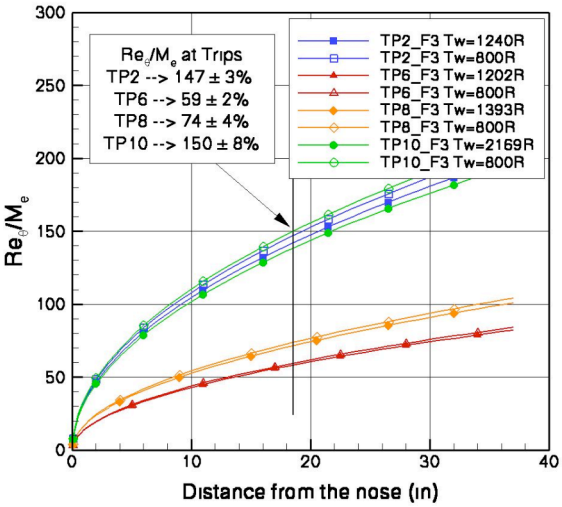

Figure 31. Mach 10 Reynolds number ratio calculations at the trip station

which corresponds to a k/δ range of 65 to 79%. Based on the present analysis (which purposefully mimicked the design approach) the boundary layer trip height to boundary layer ratio was within the target range and the trips performed as designed for the Mach 7 flight.

Figure 31 provides the calculated Re_θ/M_e as a function of the lower surface axial distance for the Mach 10 trajectory points associated with T201. As revealed in Fig. 20, TP2 and TP10 correspond to when the trips were shown to be fully effective (turbulent at the furthest forward measurement location, T201), while TP6 and TP8 correspond to when the trip were shown not to be fully effective (not turbulent at T201). The calculations reveal a distinct shift in Re_θ/M_e between those two groupings. The actual values for the trip location, based on a consistent wall temperature value of 800°R, were 147, 59, 74, and 150 for trajectory points 2, 6, 8, and 10, respectively. When considering the sensitivity of these calculations to the measured wall temperature variations, at worst an 8% difference was observed.

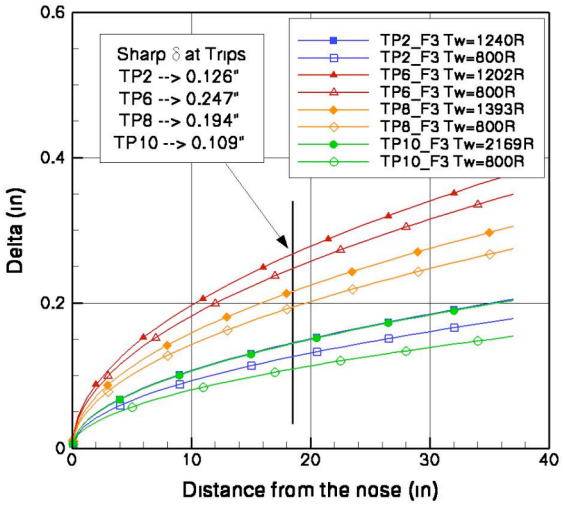

Figure 32. Mach 10 boundary layer thickness calculations at the trip station

The corresponding boundary layer thickness calculations for the T201 Mach 10 trajectory points are shown in Fig. 32. While the groupings in this case are not as distinct, nevertheless the trends suggest a δ threshold, above which the trips are no longer fully effective. As noted previously, these calculations are for a sharp leading edge and a bluntness increment is needed to compare against the pre-flight predictions that were used to size the Mach 10 trips. At present, a Mach 10 bluntness increment has not been finalized, partially due to the fact that the nose bluntness of the flight vehicle had changed just prior to flight, and thus the pre-flight calculations to size the Mach 10 trips are not consistent with our present calculations. But a rough comparison of pre-flight to present calculations suggests a bluntness increment on the order of 0.12-in, which then corresponds to a k/δ of order one being the threshold for when the trips were no longer effective, in qualitative agreement with the simple design philosophy used to size the Mach 10 trips. In other words, based on the local conditions at the trip, when the trip height was appreciably below the boundary layer thickness for the Mach 10 flight, the trips were no longer fully effective, which was consistent with the ground-based findings[7].

VI. Conclusion

The successful Mach 7 and 10 Hyper-X flights have provided the opportunity to assess the rationale and methodologies utilized during the design of the flight vehicles. One decision made early in the design process was to use boundary layer trips ahead of the inlet to force transition and reduce susceptibility to flow separations in front of and within the scramjet engine. The flight instrumentation layout was selected to provide enough coverage and redundancy to be able to determine and assess the vehicle flight performance. In this case, the surface thermocouple data from the both flights were used to assess the boundary layer state during each trajectory, both on the lower surface to determine trip effectiveness, and on the upper surface to evaluate the natural transition state of the vehicle. The present paper provides a brief review of the ground-based trip design effort, a presentation of the Mach 7 and Mach 10 flight thermocouple results, an analysis of the temperature-time histories to provide heating rates for determination of the times at which boundary layer transition occurred, and an assessment of the boundary layer properties that correspond to those key points along the trajectory. The present analysis has shown for both flights that the lower surface trips performed as expected based on the ground-based program and that the approach taken to scale the trips to flight was acceptable. The upper surface analysis revealed that the pre-flight hypersonic transition criteria of momentum thickness Reynolds number over the edge Mach number of 300 was a reasonable estimate of transition onset and as such the pre-flight decision to utilize trips on the lower surface was warranted.

References

1. Rausch, V. L., McClinton, C. R., and Crawford, J. L., ***Hyper-X: Flight Validation of Hypersonic Airbreathing Technology***, ISABE Paper 97-7024, 1997.

2. Rausch, V. L., McClinton, C. R., and Hicks, J. W., ***NASA Scramjet Flights to Breath New Life into Hypersonics***, *Aerospace America*, Vol. 35, No. 7, 1997, pp. 40-46.
3. McClinton, C. R., Holland, S. D., Rock, K.E., Engelund, W. C., Voland, R.T., Huebner, L. D., and Rogers, R. C., ***Hyper-X Wind Tunnel Program***, AIAA Paper 98-0553, 1998.
4. Ferlemann, S.M.; Voland, R.T.; Cabell, K, Whitte, D.; and Ruf, E., ***Hyper-X Mach 7 Scramjet Pretest Predictions and Ground to Flight Comparison,*** AIAA 2005-3322. Presented at 13th International Space Planes and Hypersonic Systems and Technology Conference, Capua, Italy. May 2005.
5. Engelund, W. C., and Holland, S. D., ***Hyper-X / X-43A Aerodynamics: Results from the Mach 7 and Mach 10 Scramjet Flight Tests***, Presented at 28th JANNAF Airbreathing Propulsion Subcommittee Meeting, Charleston, SC, June 13-17, 2005.
6. Voland, R.T and McClinton, C.R., ***NASA Hypersonic Overview***, Presented at 28th JANNAF Airbreathing Propulsion Subcommittee Meeting. Charleston, SC, June 13-17, 2005.
7. Berry SA, Auslender AH, Dilley AD, and Calleja JF. ***Hypersonic Boundary Layer trip Development for Hyper-X***. *J. Spacecr. Rockets 38(6): 853-864.*
8. Lau, K. Y., and Vaporean, C. N., ***Parametric Boundary Layer Transition Study for NASP-like Configuration Using Linear Stability Analyses,*** Presented at the National Aerospace Plane Mid-term Technology Review, Monterey CA, paper number 283, 1992.
9. Dilley, A. D., ***Hyper-X Trip Sizing and Preliminary Drag Estimates***, *Hyper-X Technical Note 96HN0064, NAS1-19864* 1996.
10. Stetson, K. F., Thompson, E. R., Donaldson, J. C., and Siler, L. G., ***Laminar Boundary Layer Stability Experiments on a Cone at Mach 8, Part 2: Blunt Cone***, AIAA Paper 84-0006, 1984.
11. Reshotko, E., ***Boundary Layer Stability and Transition***, Annual Review of Fluid Mechanics, Vol. 8, 1976, pp. 311-349.
12. Dilley, A. D., ***Final Design for Mach 7 Hyper-X Boundary Layer Trips***, Hyper-X Technical Note 99-282, NAS1-96013, 1999.
13. Huebner, L. D., and Rood, R. L., ***Instrumentation and Measurement for the Hyper-X Flight Vehicle***, JANNAF CS/PSHS/APS Joint Meetings, West Palm Beach, FL, October 1997.
14 Scott Berry, Kamran Daryabeigi, Aaron Auslender, and Robert Bittner, **Boundary Layer Transition on X-43A Flight 2**, Presented at JANNAF 28th Airbreathing Propulsion Subcommittee Meeting in Charleston, SC, June. 2005.
15. Williams, S. D., and Curry, D. M., ***Thermal Protection Systems***, NASA RP-1289, December 1992.
16. Chiu, S. A., and Pitts, W. C., ***Reusable Surface Insulations for Reentry Spacecraft***, AIAA Paper 1991-0695, January 1991.
17. Bouslog, S. A., and Cunnington, G. R., Jr., ***Emittance Measurements of RCG Coated Shuttle Tiles***, AIAA 1992-0851, January 1992.
18. Anderson, D. A., Tannehill, J. C., and Pletcher, R. H., ***Computational Fluid Mechanics and Heat Transfer***, Hemisphere Publishing, Washington, 1984.
19. Throckmorton, D. A., and Hartung, L. C., ***Space Shuttle Orbiter Entry Lee-Side Heat-Transfer Data STS-28***, NASA RP 1306, September 1993.
20. Smith, S. A., ***Digital Signal Processing, A Practical Guide for Engineers and Scientists***, Elsevier Science, Burlington, MA, 2003.
21. Daryabeigi, K., Berry, S. A., Horvath, T. J., and Nowak, R. J., ***Finite Volume Numerical Methods for Aeroheating Rate Calculations From Infrared Thermographic Data***, AIAA 2003-3634, June 2003.
22. Engel, C. D., and Praharaj, S. C., "Miniver Upgrade for the AVID System, Vol. I: LANMIN User's Manual," NASA CR-172212, Aug. 1983.
23. Baranowski, L.C., "Influence of Cross-flow on Windward Centerline Heating," MDC E0535, Dec. 1971.
24. Wurster, K.E., and Stone, H.W., ***Aerodynamic Heating Environment Definition/Thermal Protection System Selection ofr the HL-20***, *Journal of Spacecraft and Rockets*, Vol. 30, No. 5, 1993, pp. 549-557.
25. Tartabini, P. V., Wurster, K. E., Korte, J. J., and Lepsch, R. A., ***Multidisciplinary Analysis of a Lifting Body Launch Vehicle***, *Journal of Spacecraft and Rockets*, Vol. 39, No. 5, 2002, pp. 788-795.
26. Wurster, K.E., Riley, C. J., and Zoby, E. V., ***Engineering Aerothermal Analysis for X-34 Thermal Protection System Design***, *Journal of Spacecraft and Rockets*, Vol. 36, No. 2, 1999, pp. 216-228.
27. Zoby, E. V., Thompson, R. A., and Wurster, K. E., ***Aeroheating Design Issues for Reusable Launch Vehicles – A Perspective***, AIAA Paper 2004-2535, June 2004.
28. Eckert, E.R.G., "Survey of Boundary Layer Heat Transfer at High Velocities and High Temperatures," WADC, April 1960, Tech. Rept. 59-524.
29. Anderson, E.C. and Lewis, C.H., ***Laminar or Turbulent Boundary-Layer Flows of Perfect Gases or Reacting Gas Mixtures in Chemical Equilibrium***, NASA CR-1893, October, 1971.
30. Johnson, K., ***Hyper-X Aerodynamics and Propulsion Reference Systems***, Hyper-X Program Office, HX-241-Rev. A, June 1, 2004.
31. Bittner, R., ***X-43A Second Flight Boundary Layer Analysis Based on the Best Estimated Trajectory Version 2.2 (Rev A)***, Technical Note 05-453A (NNL07AA00B), NASA Langley Research Center, Feb. 28, 2008.
32. Karlgaard, C., ***X-43A Flight 2 Best Estimated Trajectory***, HX-DFRC-0389, Rev. A, Jan 31, 2005.
33. DelCorso, J., ***X-43A Flight 3 Data Release (Attachment 3)***, HX-1077, May 2005.
34. Auslender, A., Berry, S., and Dilley, A., ***Boundary Layer Trip Selection/Design for the Mach 7 Hyper-X Research Vehicle (HXRV)***, Hyper-X Program Office, HX-721, September, 1999.